Check for updates

OPEN

Comprehensive analysis of reservoir comparison and controls on pore structure in the Wufeng-Longmaxi shale, Southern Sichuan

Yijiang Leng[1,2], Hongming Tang[1,2✉], Yutian Feng[1,2], Xuewen Shi[1,2,3], Weiming Yu[3], Zeyan Li[1,2] & Hu Li[4]

Significant variations in depositional environments, reservoir conditions, and burial depths across the Yuxi, Luzhou, Changning, and Zhaotong areas, this study investigates the reservoir heterogeneity and pore structure controls in Sichuan Basin's Wufeng-Longmaxi shales. This paper studys the reservoir characteristics of four typical shale exploration areas, by using XRD, FE-SEM and low-temperature N_2 adsorption experiments. The main controls on pore structure were then selected using the grey correlation algorithm. High-quality shale reservoirs consistently develop at the base of the Longmaxi Formation. However, excessive thermal maturity causes degradation of hydrocarbon generation potential and storage capacity in localized areas. There is a strong correlation between pore structure and TOC content (correlation coefficient: 0.72–0.76), Ro (0.73–0.74), tectonics (0.65–0.71), and burial depth (0.23–0.63). Pore structure parameters exhibit a strong positive correlation with TOC content. Pore systems undergo a six-stage evolutionary progression with advancing thermal maturity. In structurally compromised anticlines, pore networks develop directional slit-shaped configurations with reduced pore volumes and surface areas, while excessive burial depth similarly causes reduction in these two parameters. This paper is crucial for improving an understanding of the shale pore system and facilitating the efficient development of shale gas resources.

Keywords Pore structure, Organic shale, Shale gas, Porosity evolution, Grey correlation

Shale gas, as a highly promising unconventional natural gas resource, has significantly contributed to global natural gas production in recent years[1–3]. The Wufeng-Longmaxi formations in southern China, characterized by their substantial thickness and widespread distribution, have become a focus of commercial shale gas development[4]. It has been shown that the differential development of the Wufeng-Longmaxi shale reservoir occurs under the control of various factors such as mineralogical composition, organic matter content, and structural conditions[5–7]. Covering an exploration area of 3.5×10^4 km², the shale gas reservoirs in southern Sichuan Basin exhibit pronounced lateral and vertical heterogeneity. Systematic differences among different blocks in terms of sedimentary facies, structural background, reservoir conditions and engineering mechanics characteristics, which leads to significant zonal characteristics in the gas bearing capacity and final output in the development practice. Through technological breakthroughs, profitable large-scale development has been achieved in mid-depth areas (predominantly burial depth < 3500 m), exemplified by the Changning and Weiyuan areas. Concurrently, deep areas (3,500–4,500 m) represented by Luzhou and Yuxi areas have yielded high-flow breakthroughs in multiple shale gas wells[8]. It demonstrates an integrated advancement pattern with coordinated breakthroughs across southern Sichuan's shale gas plays. However, these studies predominantly focused on localized well areas or specific stratigraphic intervals, neglecting the broader spatial variations in reservoir characteristics. The Wufeng-Longmaxi shale, characterized by early Paleozoic deposition, has undergone multiple tectonothermal events including the Caledonian, Indosinian, Yanshanian, and Himalayan orogenies. Consequently, pronounced variations exist in burial depth, structural deformation intensity, and thermal maturity across the formation[9,10].

[1]School of Geoscience and Technology, Southwest Petroleum University, Chengdu 610500, China. [2]Natural Gas Geology Key Laboratory of Sichuan Province, Southwest Petroleum University, Chengdu 610500, China. [3]Shale Gas Research Institute, PetroChina Southwest Oil & Gasfield Company, Chengdu 610051, China. [4]School of Economics, Sichuan University of Science and Engineering, Yibin 644000, China. ✉email: tanghm@swpu.edu.cn

This study addresses these knowledge gaps by analyzing samples from the Wufeng-Longmaxi Formation in four distinct areas (Yuxi, Luzhou, Changning and Zhaotong). Through a detailed characterization of geological features across different areas and layers, combined with various experimental techniques, this research aims to elucidate the diverse characteristics of the shale reservoir. Utilizing a grey correlation algorithm, the study comprehensively analyzes and optimizes the primary controlling factors of nanoscale pore structure within the shale. The findings clarify the impact of various factors on the shale pore system and establish a model for the cooperative development and evolution of organic-inorganic pore systems in shale. This research provides a theoretical foundation for further evaluation and optimization of favorable shale reservoir areas.

Geological setting

The Sichuan Basin, situated in the Upper Yangtze region, has undergone a complex history of multi-stage and multi-directional tectonic movements. The basin is divided into six secondary structural units and represents the largest unconventional gas exploration and development zone in China[11]. The study area, located within the southern Sichuan Basin, is characterizes by the widespread distribution of marine organic-rich shales of Wufeng-Longmaxi formations. This region encompasses a diverse range of shale gas reservoirs, including deep gas reservoirs (> 3500 m) in Yuxi and Luzhou, middle-deep reservoirs (2000–3500 m) in Changning, and middle-shallow reservoirs (500–2000 m) in Zhaotong (Fig. 1a).

The Upper Ordovician Wufeng-Lower Silurian Longmaxi formations exhibit continuous development, with a distinctive shell marl layer (0.5–2.5 m) of the Guanyinqiao Formation commonly interbedded between them. Based on sedimentary cycles, the Longmaxi Formation can be further subdivided into S_1l and S_2l Subformations. The S_1l Subformation predominantly comprised gray-black shale and can be divided into S_1l_1 and S_1l_2 Members. The basal portion of the S_1l_1 Member, specifically the $S_1l_1{}^1$-$S_1l_1{}^3$ layers, is characterized by dark gray-black organic-rich shale, abundant graptolites and laminae. These layers currently constitute the primary target for exploration and development within the Wufeng-Longmaxi formations (Fig. 1b).

Samples and methods
Samples

To ensure comparability of experimental results, 92 shale samples were collected from 11 wells within the Wufeng-Longmaxi formations in the Yuxi, Luzhou, Changning and Zhaotong areas of the Sichuan Basin, southern China (Fig. 1a).
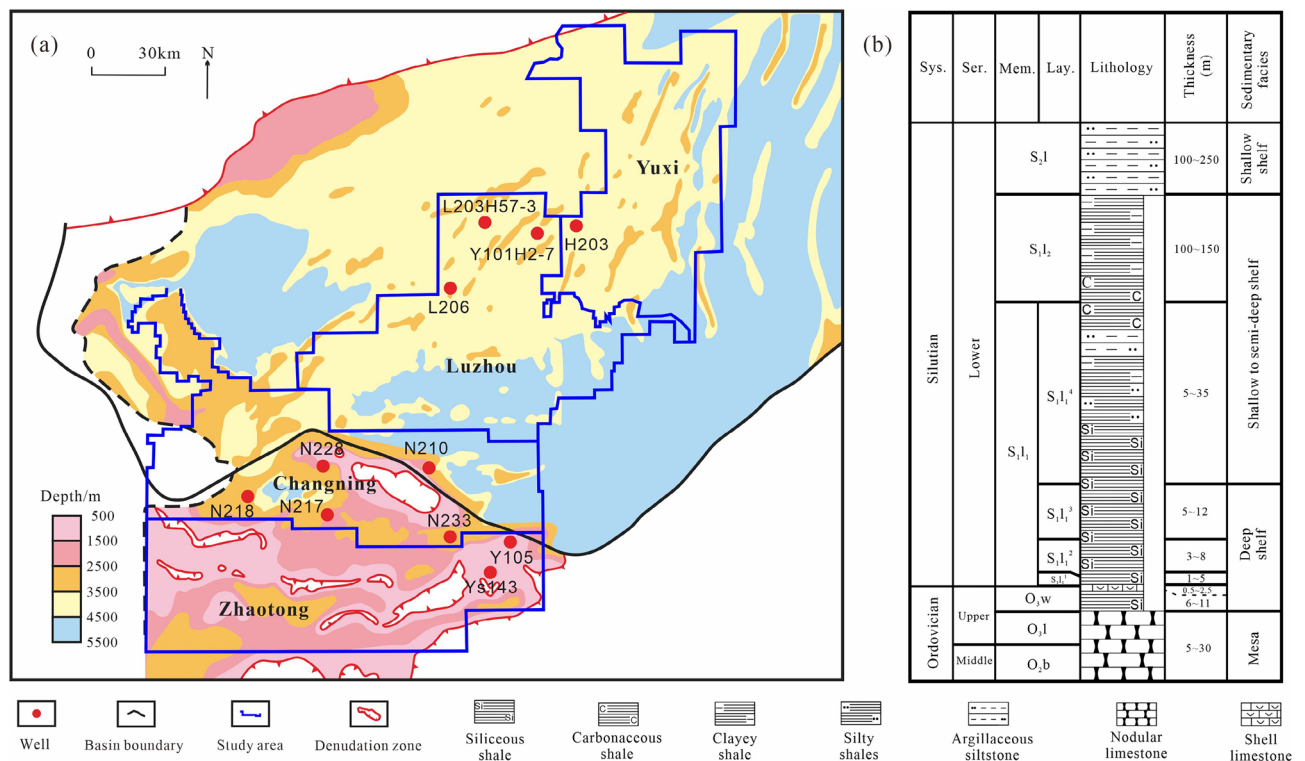

Fig. 1. (**a**) Burial depth of the Wufeng Formation (bottom) in the southern Sichuan Basin, showing the location of the study areas and wells (modified from[3]). (**b**) Lithostratigraphic column and the depositional environment of the Middle Ordovician-Lower Silurian sedimentary sequence in the Sichuan Basin.

Experiments and methods

X-ray diffraction, total organic carbon content, and porosity
X-ray diffraction (XRD) analysis was conducted using a BRUKER D8 ADVANCE X-ray diffractometer, following the SY/T 5163 – 2010 standard. Total organic carbon (TOC) content was determined using a CS230SH carbon-sulfur analyzer, adhering to the GB/T 18,602 – 2012 Chinese national standard method. Porosity was measured using an HP-40 shale helium porosity analyzer, in accordance with the GB/T 34,533 – 2023 Chinese national standard method.

Vitrinite reflectance (Ro)
Vitrinite reflectance (Ro) was estimated using an empirical formula conversion based on the reflectance of asphalt[12]. The calculation formula is as follows:

$$Ro = 0.618Rb + 0.40 \qquad (1)$$

where *Rb* represents the reflectance of shale asphalt, %; and *Ro* is equivalent vitrinite reflectance, %.

The experimental process strictly complies with GB/T 6948 – 2008. Samples underwent necessary pretreatment to prepare standard polished blocks, mounted in epoxy resin and polished to a mirror finish; During testing, 30 measurement points were randomly selected per sample for Ro analysis; A data validity threshold was set at ≤ 0.5% variance in reflectance per sample (to exclude outlier interference).

Field emission scanning electron microscopy (FE-SEM)
Shale samples were initially polished with a LEICA EM TIC3X ion milling system to obtain optically smooth surfaces and ensuring high-quality image acquisition. Subsequently, the morphology, size, and distribution characteristics of the pore-fracture system were observed using a FEI Quanta 650 FEG environmental scanning electron microscope, following the SY/T 5162 – 1997 standard.

Low-temperature N_2 adsorption
Low-temperature N_2 adsorption analysis was performed using a Micromeritics Autosorb IQ automatic specific surface area and porosity analyzer. Prior to measurement, all shale samples were degassed at 110 °C for 8 h under vacuum to remove moisture and adsorbed contaminants. The analysis was conducted at 77 K over a relative pressure range from 0.01 to 0.995, adhering to the SY/T 6154 – 1995 Chinese oil and gas industry standard. The BJH (Barrett-Joyner-Halenda) and DFT (Density Functional Theory) models were employed to characterize pore structure parameters.

Results

Mineralogical composition and porosity

Table 1 presents the mineralogical composition and porosity of shale samples collected from four representative wells. The porosity values range from 2.41 to 6.94%, with an average value of 4.09%. The mineralogical composition is dominated by quartz and clay minerals, with average contents of 45.5% and 25.8%, respectively.

Sample ID	TOC (%)	Porosity (%)	Mineral composition (%)					
			Quartz	Feldspar	Calcite	Dolomite	Pyrite	Clay
H-1	2.35	2.68	43.7	6.0	9.3	6.7	2.7	31.6
H-2	4.07	4.06	56.7	3.1	1.2	3.2	6.4	29.4
H-3	4.16	2.94	66.7	2.2	7.7	6.9	3.0	13.5
H-4	2.38	2.41	37.8	3.8	0.0	17.0	3.2	38.2
L-1	2.33	3.29	24.7	11.6	10.7	6.0	10.1	35.8
L-2	3.56	3.88	78.9	3.4	1.4	2.1	2.4	11.8
L-3	4.41	4.28	58.6	4.4	6.5	8.7	3.4	18.4
L-4	4.07	5.29	56.2	4.3	13.2	3.4	4.0	18.9
L-5	0.18	3.34	28.5	3.6	29.4	2.7	1.1	34.7
N-1	2.50	4.77	36.6	9.3	10.9	0.0	2.0	41.2
N-2	4.25	6.77	51.1	5.7	16.3	0.0	4.3	22.6
N-3	3.61	4.58	69.8	2.9	10.9	2.9	2.0	11.5
N-4	4.93	6.94	55.5	4.5	15.1	8.8	3.4	12.7
N-5	2.62	4.34	33.8	3.7	24.9	10.7	1.3	25.6
Y-1	1.90	3.27	28.1	4.2	14.9	14.2	3.8	34.8
Y-2	2.37	3.13	38.0	2.9	17.1	8.2	5.2	28.6
Y-3	2.76	4.28	35.7	3.7	17.3	12.3	4.1	26.9
Y-4	4.20	4.51	36.2	5.0	14.4	13.2	5.0	26.2
Y-5	2.30	2.96	28.3	1.1	29.7	11.0	2.7	27.2

Table 1. The TOC, porosity and mineralogical composition of shale samples.

Feldspar, calcite, dolomite, and pyrite are present in relatively lower proportions, with average contents of 4.5%, 13.2%, 7.3% and 3.7%, respectively. The higher content of siliceous minerals (feldspar and quartz) is beneficial for pore preservation and, in combination with carbonate minerals (calcite and dolomite), contributes to reservoir brittleness. During hydraulic fracturing, these brittle minerals promote the formation of complex fracture networks, thereby improving reservoir stimulation efficiency and ultimately increasing gas production. In contrast, clay minerals exhibit a strong adsorption capacity for shale gas, leading to a large specific surface area in shale reservoirs with high clay mineral content. This provides more adsorption sites for shale gas, potentially influencing the gas content of shale reservoirs. Overall, the $S_1l_1^1$-$S_1l_1^3$ layers at the base of the Longmaxi Formation demonstrate a higher content of brittle minerals and exhibit higher porosity, making them the most favorable layers for exploration and development.

Organic geochemical characteristics

Total organic carbon content

TOC content serves as a fundamental indicator of shale's hydrocarbon generation potential and plays a significant role in the development of organic pores. During the deep water sedimentation of the Wufeng-Longmaxi formations, two sedimentary centers emerged in the Sichuan Basin. Wells H203, L206, and N233 are situated within the Yibin-Chongqing-Qijiang sedimentary center (Fig. 2). Black, thick shale in this area exhibits relatively high TOC content, ranging from 0.18 to 4.93% with an average of 3.24% (Fig. 3; Table 1). Well Y105 is located on the southern margin of Sichuan Basin, where the influence of the Central Guizhou Paleouplift led to shallow shelf facies during the deposition of the Longmaxi Formation (Fig. 2). This well shows a relatively lower TOC content, ranging from 1.90 to 4.20% with an average of 2.71% (Fig. 3; Table 1).

A consistent longitudinal trend reveals that the $S_1l_1^1$-$S_1l_1^3$ lays exhibit higher TOC content, providing a robust material basis for substantial shale gas generation. These layers represent the primary targets for current shale gas exploration and development. While the TOC content of $S_1l_1^4$ layer, situated above the upper part of the Longmaxi Formation, is lower than that of the bottom layers, it still remains relatively high, suggesting its potential as a replacement horizon for future development.
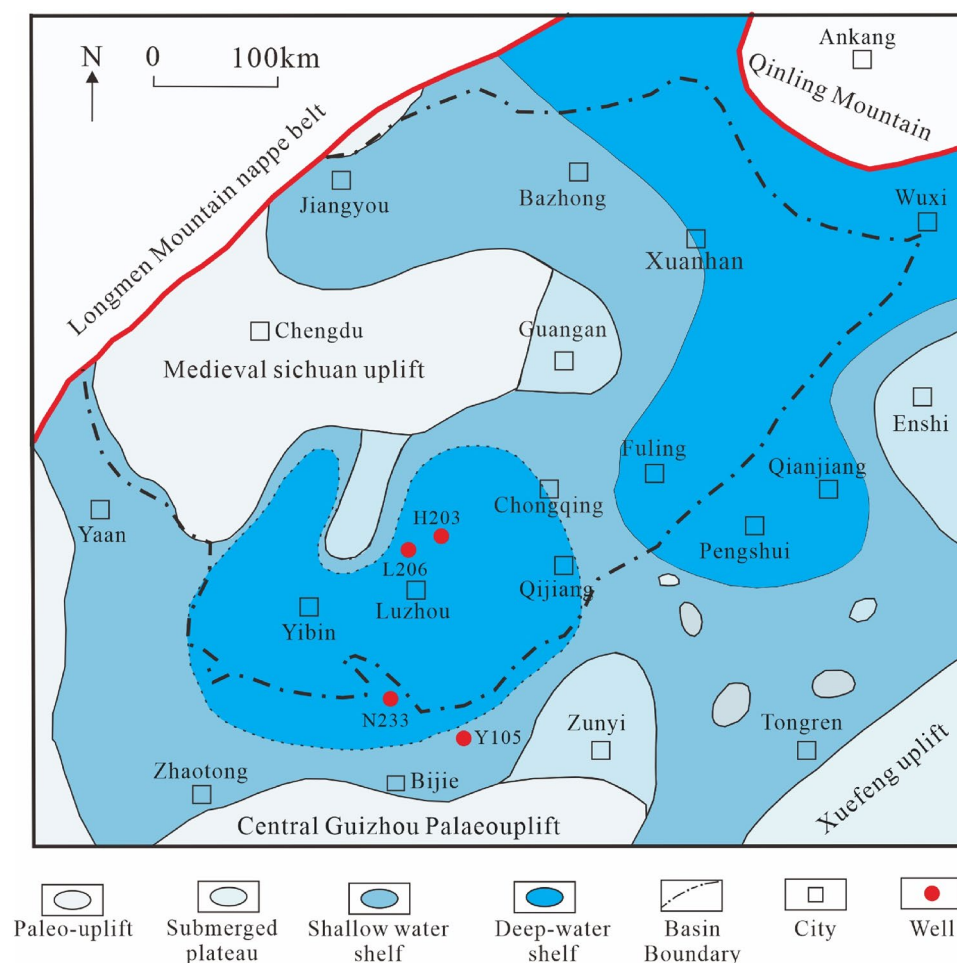

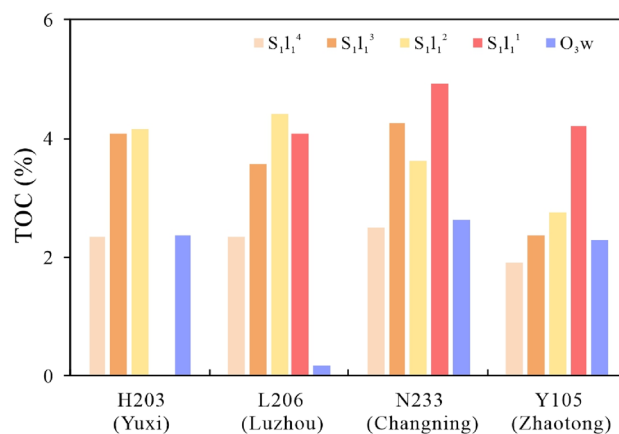**Fig. 2**. Sedimentary facies of the Longmaxi formatiaon in the Sichuan Basin and its adjacent areas (modified from[5]).

Fig. 3. Comparison of TOC content in different areas (representative wells are shown).
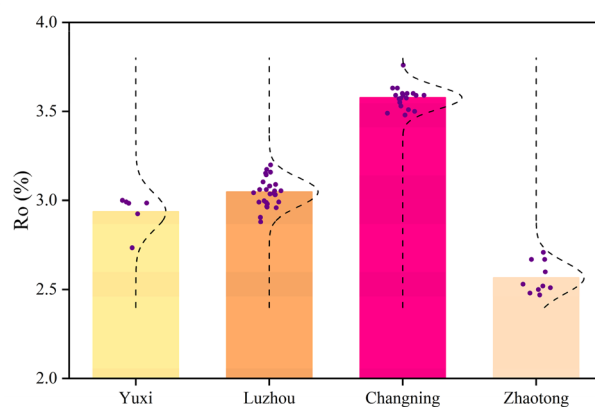

Fig. 4. Comparison of Ro in different areas (dashed lines exhibit the normal distribution of data).

Vitrinite reflectance (Ro)
The maturity of organic matter is a crucial parameter for evaluating shale gas generation potential, and it is primarily influenced by burial history and the occurrence of abnormal thermal events[13]. Compared to North America, the Ro of the Wufeng-Longmaxi shale in South China is relatively high due to the deep burial depth associated with the Yangtze Platform and the influence of the Emei Mountain igneous province[14–17]. In certain areas, organic matter has reached the late mature stage (Figs. 4 and 5). Consequently, it is essential to elucidate the relationship between Ro and shale gas generation and storage capacity in production practices and to identify potential exploration risk zone within the region.

The Ro values of shale samples analyzed in this study range from 2.47 to 3.76%, indicating that all samples fall within the over-mature stage (Fig. 4). The Zhaotong area, characterized by shallower burial depths and lower thermal evolution, exhibits Ro values ranging from 2.47 to 2.71%, with an average of 2.57%. The Yuxi and Luzhou blocks, influenced by greater burial depths, display higher Ro values ranging from 2.74 to 3.20%, with an average of 3.03%. The western portion of the Changning block, impacted by the Emei Mountain basalt, exhibits the highest thermal evolution maturity, with Ro values ranging from 3.48 to 3.76%, and an average of 3.58% (Fig. 4).

Spatially, the Weiyuan area is enclosed by regions of lower organic matter maturity within the basin, where Ro values are generally below 3.0%, with localized areas measuring less than 2.5% (Fig. 6a). Moving southeast from Weiyuan, the maximum ancient burial depth of the strata progressively increases, resulting in a gradual increase in Ro values, reaching approximately 3.5% in the Changning area (Fig. 6a). Further eastward and westward from the Changning anticline, Ro values continue to rise. The Yanjin area in the west, located within the Emei Mountain basalt zone, experiences Ro values as high as 3.8% due to the influence of magma baking (Fig. 6b). To the east, the Xuyong area exhibits the greatest paleo-burial depth within the basin, with Ro values in some localities exceeding 4.0% (Fig. 6b).

Pore structure characteristics
Low-temperature N_2 adsorption is an effective technique for characterizing the structural parameters and morphology of shale pores[18–20]. The adsorption isotherms of the 19 analyzed samples exhibit an inverse S-shape,
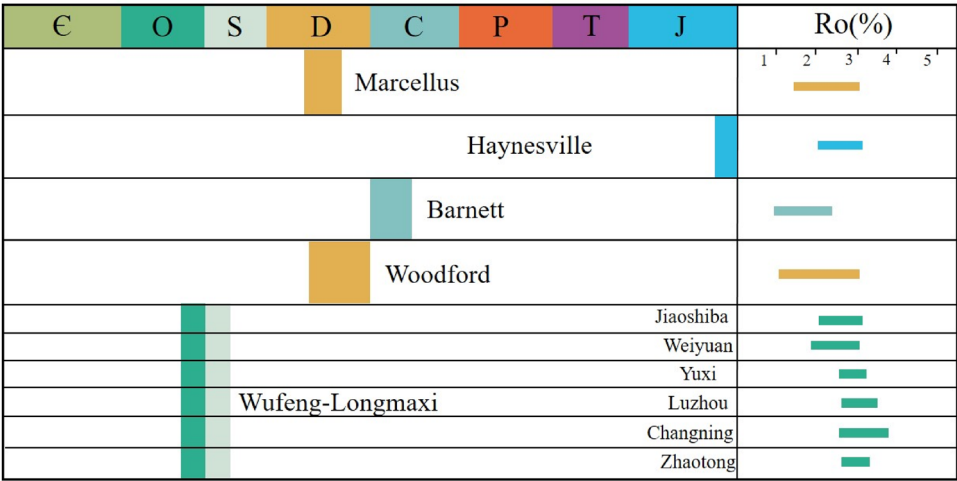
Fig. 5. Comparison of Ro values in North America and the Wufeng-Longmaxi formations across different areas (modified from[14]).
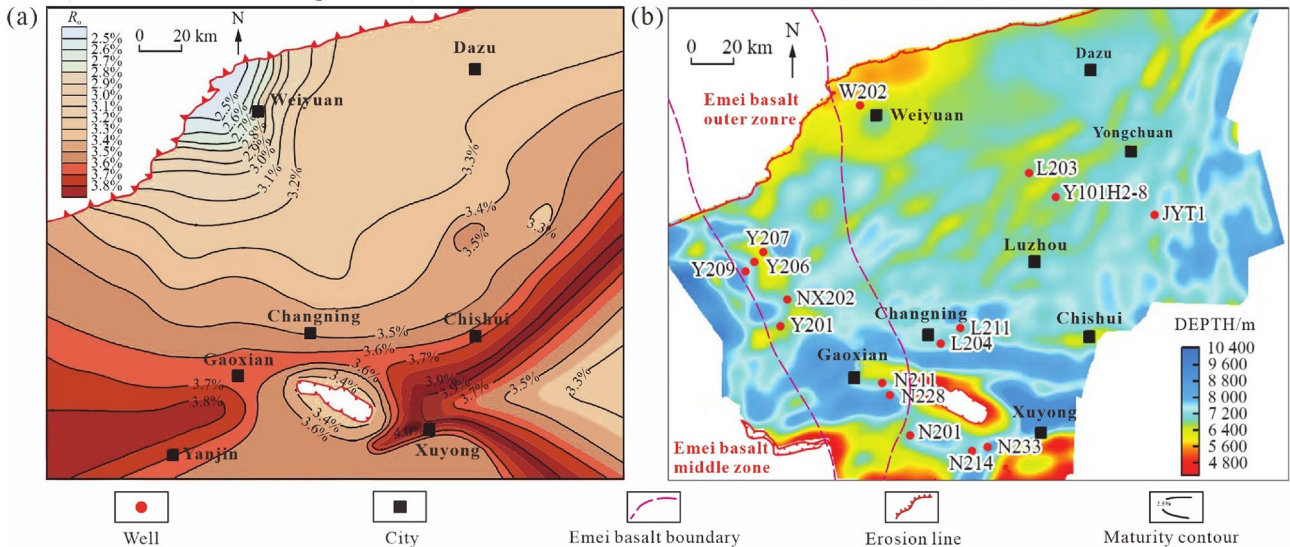

Fig. 6. (**a**) Contour map of Ro valued in the Wufeng-Longmaxi formations. (**b**) Maximum ancient burial depth of the Wufeng Formation (basal part) in southern Sichuan and Emei basalt distribution (modified according from[13]).

indicative of Type IV characteristics according to IUPAC classification[21]. The adsorption curves display distinct features across three pressure ranges: low pressure ($P/P_0 < 0.05$), medium-high pressure ($0.45 < P/P_0 < 0.95$) and high pressure ($P/P_0 > 0.95$). These correspond to micropore filling, single-layer and multi-layer adsorption stages of nitrogen molecules, respectively. As the relative pressure approaches unity, the adsorption capacity continues to increase. The desorption curve does not overlap with the adsorption curve in the medium-high pressure range ($0.45 < P/P_0 < 0.95$), resulting in a hysteresis loop. (Fig. 7). The hysteresis loops observed in the N_2 adsorption and desorption curve of the studies shale samples primarily exhibit H3 characteristics, displaying features of both H2 and H4 types. This indicates a pore system predominantly composed of ink-bottle pores with localized development of slot and slit pores (Fig. 7).

Table 2 presents the pore structure parameters of the 19 shale samples. The specific surface area of the samples ranges from 7.23 m²/g to 27.23 m²/g, with an average value of 17.81 m²/g. The pore volume ranges from 3.92×10^{-3} cm³/g to 34.01×10^{-3} cm³/g, averaging 17.06×10^{-3} cm³/g. The hysteresis coefficient, calculated as the ratio of the hysteresis area to the envelope area of the adsorption curves, provides insights into the openness and connectivity of shale pore structures[22,23]. The results reveal that shale samples from well H203 and Y105 exhibit relatively low hysteresis coefficient, averaging 0.0341 and 0.0384, respectively. This suggests a predominance of Slit pores, indicating improves connectivity and openness (Fig. 7a, d; Table 2). In contrast, samples from
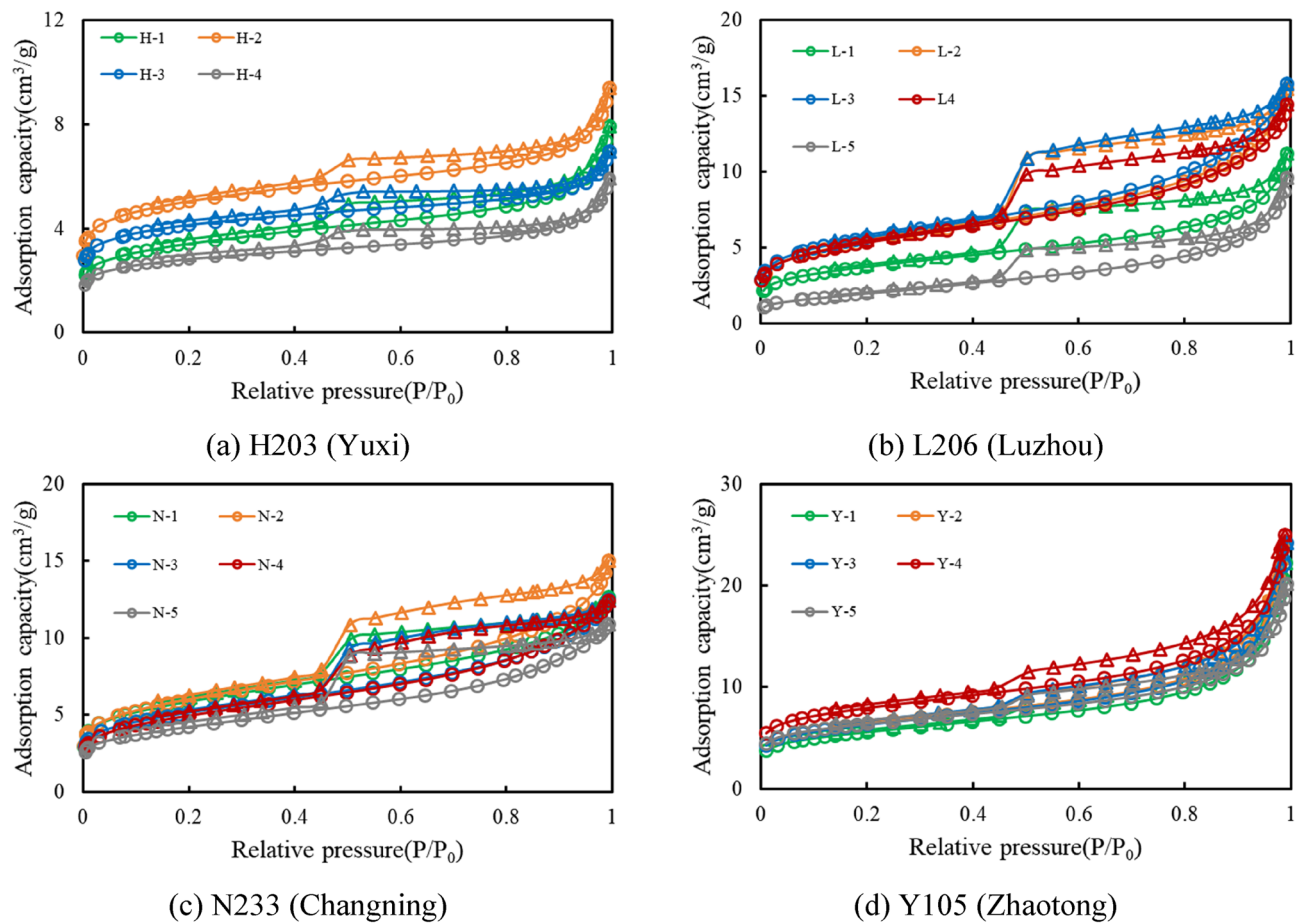
(a) H203 (Yuxi)

(b) L206 (Luzhou)

(c) N233 (Changning)

(d) Y105 (Zhaotong)

Fig. 7. N_2 adsorption and desorption curves of shale samples from different areas.

Sample ID	TOC (%)	Porosity (%)	N_2 adsorption			
			S_{BET} (m²/g)	V_{BJH} (10^{-3}cm³/g)	Hysteresis area	Hysteresis indices
H-1	2.35	2.68	12.09	6.35	0.2139	0.0516
H-2	4.07	4.06	18.06	6.10	0.0949	0.0164
H-3	4.16	2.94	14.92	3.92	0.0986	0.0214
H-4	2.38	2.41	10.12	4.43	0.1536	0.0469
L-1	2.33	3.29	13.06	10.64	0.8755	0.1737
L-2	3.56	3.88	18.89	14.23	1.3850	0.1875
L-3	4.41	4.28	19.76	14.36	1.3231	0.1705
L-4	4.07	5.29	18.61	12.84	0.9623	0.1335
L-5	0.18	3.34	7.23	11.03	0.6340	0.1941
N-1	2.50	4.77	21.06	16.26	0.7389	0.0981
N-2	4.25	6.77	21.30	18.04	1.2250	0.1545
N-3	3.61	4.58	18.36	15.79	1.0260	0.1506
N-4	4.93	6.94	17.60	16.08	0.9826	0.1470
N-5	2.62	4.34	15.12	14.11	1.0894	0.1881
Y-1	1.90	3.27	19.29	31.59	0.4419	0.0573
Y-2	2.37	3.13	22.09	34.01	0.4742	0.0543
Y-3	2.76	4.28	21.86	33.99	0.1305	0.0151
Y-4	4.20	4.51	27.23	33.45	0.6750	0.0653
Y-5	2.30	2.96	21.77	26.87	0.0012	0.0001

Table 2. N_2 adsorption and desorption pore structure parameters.

wells L206 and N233 display higher hysteresis coefficient, averaging 0.1719 and 0.1477, respectively. These samples demonstrate a greater abundance of ink bottle pores, characterized by poorer porosity connectivity and openness (Fig. 7b-c; Table 2).

Discussion
Optimizing pore structure control factors
Grey correlation multi-attribute correlation analysis theory
The grey correlation algorithm is a multi-factor statistical analysis method that assesses. Correlation based on the similarity of geometric shapes among factor curves[24,25]. The fundamental principle involves ranking evaluation indicators data according to their correlation degree following dimensionless processing. This study utilizes this method for quantitatively evaluating pore structure control factors. The analysis proceeds through the following steps.

Determining the analysis sequence   The analysis sequence comprises supersequences and subsequences. The supersequences represent the data series that reflects the system's behavior characteristics specifically, porosity, specific surface area and pore volume. Subsequence consist of factors influencing the supersequence, including TOC content, pressure coefficient, and mineralogical composition.

Let the supersequence be represented as:

$$X_0 = (x_0(1), x_0(2), x_0(3), \ldots, x_0(m)) \tag{2}$$

The subsequences are represented as:

$$(X_1, X_2, \ldots, X_n) = \begin{bmatrix} x_1(1) & x_1(2) & \ldots & x_1(m) \\ x_2(1) & x_2(2) & \ldots & x_2(m) \\ \vdots & \vdots & \ldots & \vdots \\ x_n(1) & x_n(2) & \ldots & x_n(m) \end{bmatrix} \tag{3}$$

The supersequences and subsequences can be arranged into the following matrix:

$$(X_0, X_1, \ldots, X_n) = \begin{bmatrix} x_0(1) & x_0(2) & \ldots & x_0(m) \\ x_1(1) & x_1(2) & \ldots & x_1(m) \\ \vdots & \vdots & \ldots & \vdots \\ x_n(1) & x_n(2) & \ldots & x_n(m) \end{bmatrix} \tag{4}$$

where *m* represents the number of supersequences, and *n* represents the number of subsequences.

Calculating the correlation coefficient   The correlation coefficient quantifies the correlation between the supersequence and the subsequence at each time point (the same column coordinate). It is calculated using the following formula:

$$\epsilon_i(k) = \frac{\min\min|x_0(k) - x_i(k)| + \rho \max\max|x_0(k) - x_i(k)|}{|x_0(k) - x_i(k)| + \rho \max\max|x_0(k) - x_i(k)|} \tag{5}$$

where $|x_0(k) - x_i(k)|$ represents the absolute difference between each element of the supersequence and the corresponding element of the subsequence; $\min\min|x_0(k) - x_i(k)|$ denotes the minimum absolute difference between each subsequence and the supersequence; $max max|x_0(k) - x_i(k)|$ indicates the maximum absolute difference between each subsequence and the supersequence; ρ signifies the resolution factor, which controls the sensitivity of the correlation, a smaller ρ value indicates a larger difference between correlation coefficients. Typically, ρ is set to 0.5.

Calculating the correlation degree   The correlation degree is calculated by averaging the correlation coefficients.

$$r_{0i} = \frac{1}{m} \sum\nolimits_{k=1}^{m} \epsilon_i(k) \tag{6}$$

Quantitative evaluation of pore structure control factors
The Wufeng-Longmaxi formations in the Sichuan Basin have undergone a protracted history of sedimentation, diagenesis, organic matter thermal evolution, and multiple tectonic events. These processes have resulted in the unique development of pore characteristics within the formation[26]. Extensive research by numerous experts and scholars has investigated the factors influencing shale pore structure. It is widely recognized that various factors, including mineralogical composition, organic matter type, content, and maturity, as well as tectonic deformation, play significant roles in shaping pore structure[27–29]. Building upon these previous studies, this paper utilizes a grey correlation algorithm to quantitatively assess the correlation coefficients between six key factors (TOC content, Ro, burial depth, pressure coefficient, tectonics and mineralogical composition) and pore structure parameters. The analysis revealed that TOC content and Ro exhibit the strongest correlation with pore structure parameters, with correlation coefficients ranging from 0.72 to 0.76, and 0.73 to 0.74, respectively.

Tectonic activity, burial depth, and pressure coefficient demonstrate moderate correlations, with coefficients ranging from 0.65 to 0.71, 0.23 to 0.63, and 0.43 to 0.55, respectively. Mineralogical composition exhibits the weakest correlation with pore structure parameters, with coefficients ranging from 0.39 to 0.46 (Fig. 8).

The grey correlation analysis highlights the dominate role of TOC content and Ro in controlling pore structure. High TOC content and appropriate Ro levels are conducive to the development of organic pores within shale. Organic matter, during hydrocarbon generation and expulsion, produces significant quantities of organic acids, which contribute to the formation of secondary pores. The integration of these secondary pores with primary pore system forms a complex organic-inorganic pore network within the reservoir, significantly influencing shale pore structure.

Tectonics, burial depth, and pressure coefficient primarily influence pore structure by controlling the preservation conditions of the pore system. In areas characterized by stable structures, the impact of compression on the pore system gradually intensifies with increasing burial depth. However, when burial depth reaches a certain threshold, the negative effect of compaction on in upper strata pores is balanced by the positive effect of formation overpressure, leading to the preservation of the pore system. In contrast, areas with complex structural features, exhibit more pronounced tectonic deformation. Strong structural extrusion can not only damage the rock framework but also induce the development of a fracture system, facilitating shale gas migration and reducing formation pressure. As a consequence, the pore system becomes more susceptible to damage and compaction.

Inorganic pores and microfractures associated with diverse minerals constitute essential elements of the shale pore system. The development and preservation of these reservoir spaces are governed by the physical and chemical properties of mineral particles, exerting a notable influence on the overall shale pore system.

Analysis of main controlling factors of pore structure

TOC content

Figure 9 illustrates the correlation analysis between TOC content and pore structure parameters in the shale samples. A positive correlation exists between TOC content and pore specific surface area, with R^2 values ranging from 0.4230 to 0.7751 (Fig. 9a, d, g, j). This indicates a significant contribution of organic matter content to the specific surface area of shale samples. As TOC content increase, a greater abundance of organic pores develops within the reservoir, proving more adsorption sites for gas, thereby facilitating shale gas enrichment. The correlation between TOC content and pore volume exhibits variations across different areas. No discernible correlation is observed in samples from the Yuxi and Luzhou areas, with R^2 values of only 0.0003 and 0.0470, respectively (Fig. 9b, e). In contrast, the TOC content of samples from the Changning and Zhaotong areas shows a positive correlation with pore volume, with R^2 values of 0.4126 and 0.5397, respectively (Fig. 9h, k). The correlation between TOC content and porosity mirrors that observed with pore volume. The lowest correlation is found in samples from well H203 in the Yuxi area, with an R^2 value of only 0.0071 (Fig. 9c). Well L206 in the Luzhou area shows a moderate correlation with an R^2 of 0.3176 (Fig. 9f). Conversely, significant positive correlation between TOC content and porosity is evident in samples from wells N233 and Y105 in the Changning and Zhaotong areas, respectively, with R^2 values of 0.4681 and 0.8679 (Fig. 9i-l).

These finding suggest that the influence of TOC content on pore structure is not uniform across all areas. Well H203 situated in a compressional anticlinal zone, has experienced significant tectonic deformation, leading to pore crushing and diminished impact of organic matter on the pore structure. Additionally, the deeper burial depths of the samples from the Luzhou and Yuxi areas have subjected them to substantial compaction by overlying strata, resulting in some degree of compaction-induced pore damage, and a weakened influence of organic matter on pores development.

It is noteworthy that previous studies have observed non-monotonic trend in of pore structure parameters with increasing TOC content[30–32]. In these studies, a negative impact on the pore system was observed beyond a certain TOC threshold, leading to a decrease in pore structure parameters. However, this phenomenon was
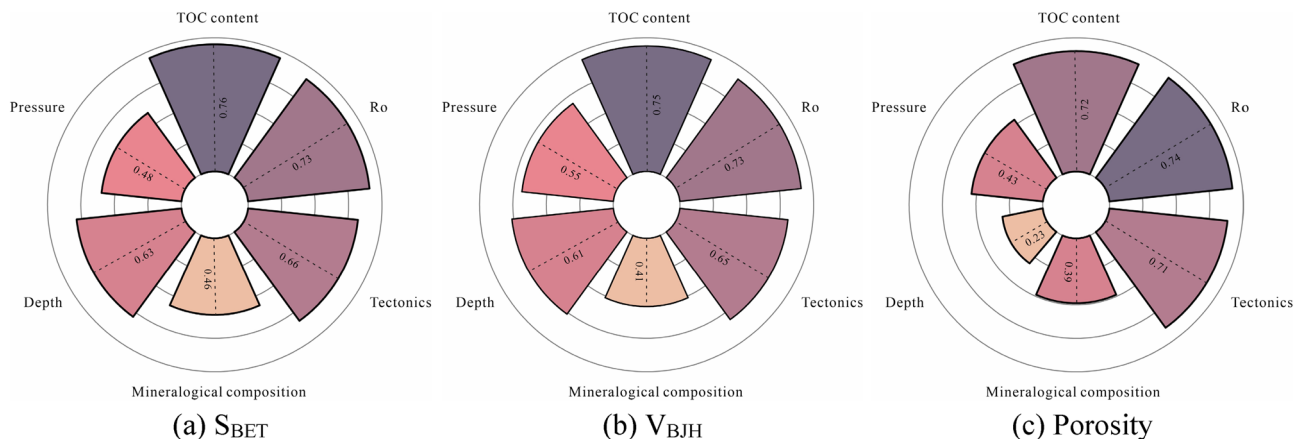

Fig. 8. Quantitative evaluation of correlation coefficients between pore structure parameters (S_{BET}, V_{BJH} and porosity) and control factors (TOC content, Ro, pressure, depth, tectonics, and mineralogical composition).
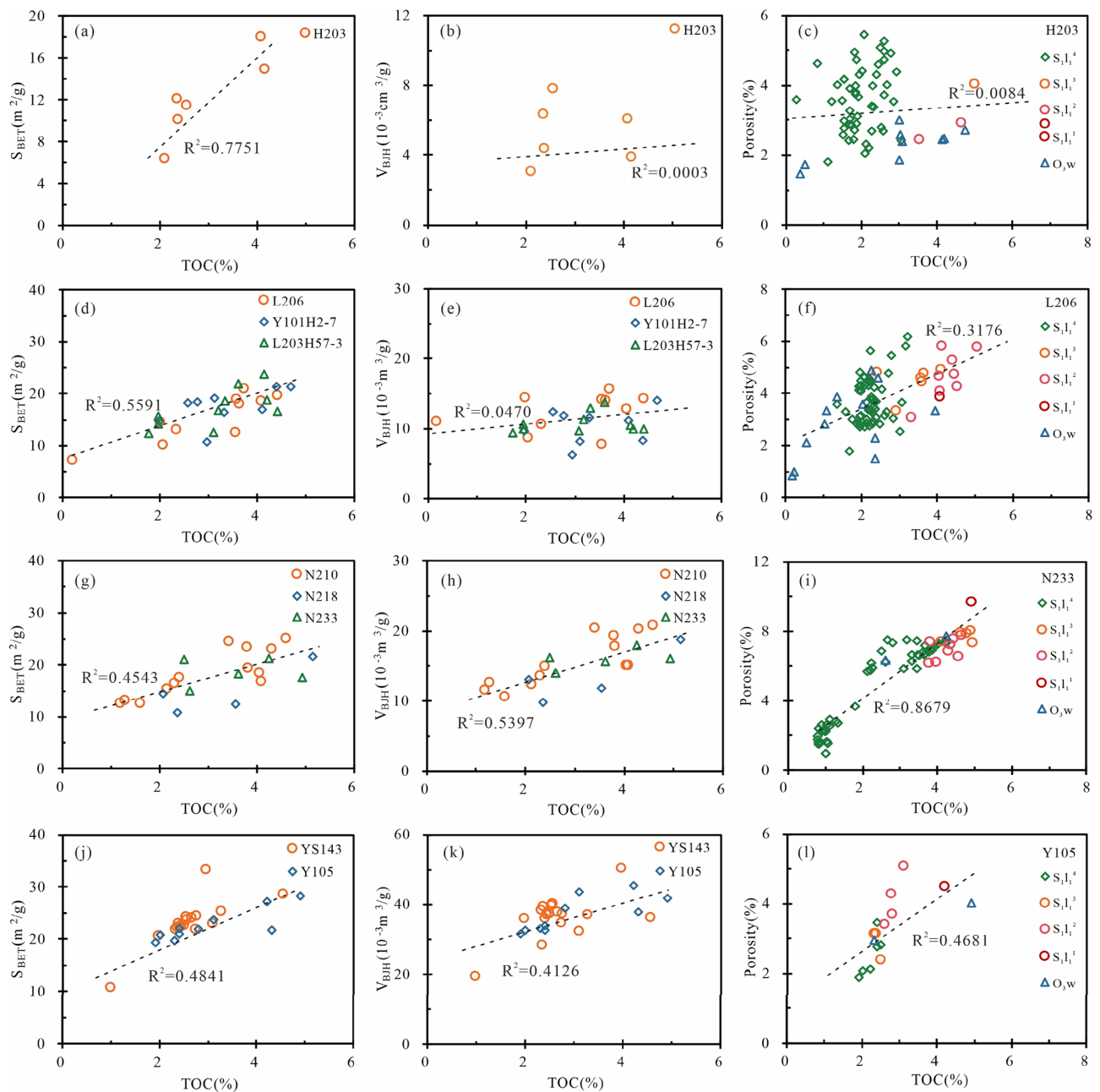
Fig. 9. Cross plots of shale pore structure parameters (S_{BET}, V_{BJH} and porosity) against TOC content in the Yuxi (**a–c**), Luzhou (**d–f**), Changning (**g–i**), and Zhaotong areas (**j–l**).

not evident in the current study. While TOC content undeniably plays a significant role in controlling the shale pore system, a comprehensive understanding requires considering the interplay between TOC content and other fundamental geological factors, such as organic matter type, Ro, and tectonics. Moreover, a holistic analysis incorporating the co-evolution model of organic-inorganic pores is essential for a comprehensive evaluation of the shale pore system.

Vitrinite reflectance (Ro)
Ro serves as a critical parameter governing the development and evolution of pore systems in shale reservoirs. Previous studies have extensively investigated the correlation between Ro and pore characteristics within the Wufeng–Longmaxi shale in southern Sichuan[33–35]. Integrating these existing findings with experimental results from this study, we propose a evolutionary model of the pore system across a maturity spectrum ranging from immature to overmature conditions. Based on progressive organic matter maturation, the evolution of the shale pore system can be classified into six distinct stages (Table 3).

Ro	Stage	Variation characteristics of the pore system	Pore structure parameter
<0.5%	Initial deposition	Progressive increase in burial depth induces mechanical compaction of pore systems.	Decrease
0.5–0.65%	Initial development	Kerogen pyrolysis develops organic pores during hydrocarbon generation; Organic acid dissolution of minerals creates secondary porosity.	Increase
0.65–1.15%	Rapid reduction	Residual liquid hydrocarbons and pyrolytic solid bitumen infill pore systems.	Decrease
1.15–2.0%	Massive development	Kerogen and bitumen pyrolysis develops organic pores; Gas-phase conversion of liquid hydrocarbons induces pore reopening; Smectite-to-illite conversion yields clay-mineral intergranular pores.	Increase
2.0–3.5%	Stable development	Hydrocarbon generation-induced porosity counteracts the destructive effects of mechanical compaction, leading to an equilibrium in pore system evolution	Stably developed
>3.5%	Graphitization	Graphitization of organic matter induces structural collapse of pore systems.	Decrease

Table 3. Six-stage evolutionary characteristics of pore structure parameters with Ro.

The analysis reveals that the effect of Ro on pore structure parameters is controlled by a dynamic coupling of organic and inorganic co-evolution, incorporating hydrocarbon generation, diagenetic processes, and burial history. The evolutionary characteristics of the pore system through the six distinct stages are outlined below.

Initial deposition stage (Ro < 0.5%)   During this stage, characterized by shallow burial, organic matter remains immature. A limited amount of biogenic gas is generated under the influence of surface organisms. The pore system primarily consists of inorganic pores within the originally deposited mineral particles, along with a small number of organic pores developed within surface organisms. As burial depth increases, the pore system undergoes significant mechanical compaction, leading to a rapid decrease in pore structure parameters.

Initial development of the pore system (0.5% < Ro < 0.65%)   Upon entering the early mature stage, organic matter reaches the oil generation window and begins to undergo cracking, producing hydrocarbons. This process marks the onset of organic pore formation. Simultaneously, the release of organic acids during hydrocarbon generation dissolves mineral particles, leading to the formation of additional secondary pores. The combined effect of these process results in a minor increase in pore structure parameters during this stage.

Rapid reduction of the pore system (0.65% < Ro < 1.15%)   As hydrocarbon generation progresses, the generation of significant amounts of liquid hydrocarbons and solid bitumen from kerogen leads to substantial filling and plugging of the shale pore system, resulting in a considerable decrease in pore structure parameters.

Massive development of the pore system (1.15% < Ro < 2.0%)   This stage represents a critical period for pore system formation. The further increase in the thermal evolution of organic matter culminates in peak hydrocarbon generation. Kerogen and bitumen release substantial hydrocarbons, forming numerous pores. Simultaneously, the transformation of liquid hydrocarbons into gaseous hydrocarbons occurs, leading to the reopening of pores that were previously blocked. Moreover, the interaction between organic acids and feldspar-carbonate minerals results in the formation of dissolution pores. Additionally, the transformation of montmorillonite to illite leads to volume contraction, creating intercrystalline pore with clay minerals. During this stage, the shale pore system undergoes rapid development due to the combined influence of various favorable factors, significantly enhancing pore structure parameters and reservoir properties.

Stable development of the pore system (2.0% < Ro < 3.5%)   Hydrocarbon generation reaches a plateau during this stage, and the growth rate of organic pores gradually declines. Simultaneously, continued burial depth increases contribute to compaction-induced pore destruction. The interplay of these factors leads to a relatively stable shale pore system, with minimal changes in pore structure parameters.

Graphitization stage (Ro > 3.5%)   As organic matter enters the advanced overmature stage, its carbon atom structure transitions from a disordered to an ordered arrangement, ultimately forming an anisotropic graphite structure. This process leads to the collapse and reduction of organic pores, resulting in a significant decrease in pore structure parameters. Consequently, the shale reservoir loses its exploration and development value (Fig. 10).

Tectonics
In addition to the previously discussed factors, the Ordovician Wufeng-Silurian Longmaxi formations in the Sichuan Basin have undergone multiple-stages of tectonic uplift, significantly influencing the development and preservation of shale reservoirs. As a result, shale pore structures exhibit notable variations across different tectonic settings[29,36].

To illustrate these variations, wells H203 and L206, located in contrasting structural settings, were selected for analysis. Well H203, situated near the core of an anticline, has experienced intense tectonic compression. Multiple stages of tectonic fractures, primarily filled with calcite and characterized by a millet ridge morphology, are evident within the core (Fig. 11a). Well L206, located in the synclinal core, is situated further from major faults and exhibits relatively stable tectonic conditions. The core remains intact, with clear bedding structures and only a few tensile fractures present (Fig. 11d). FE-SEM images reveal that pores in well H203 have
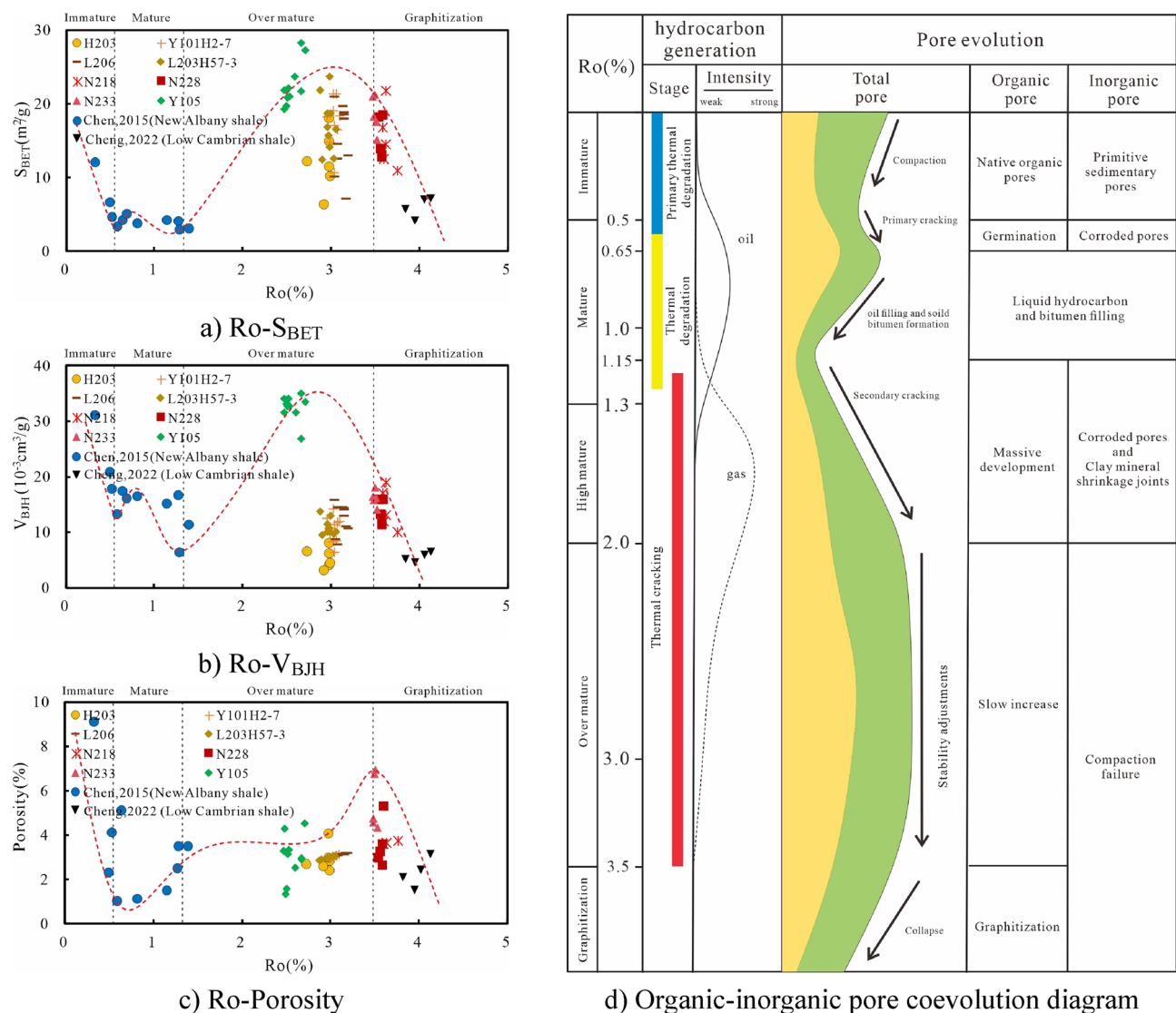
Fig. 10. Variation trends of shale pore structure parameters with Ro (Data from the NewAlbany shale in North America and the Lower Cambrian shale in Southern China are included for comparison).

undergone significant deformation due to intense tectonic extrusion. The pore morphology predominantly comprises slit-shaped pores aligned along a common axis (Fig. 11b-c). The pore specific surface area, volume and porosity are relatively lower, averaging 12.2 m²/g, 5.3 × 10⁻³ cm³/g, and 3.02%, respectively (Table 2). In contrast, shale samples from well L206 display a significant abundance of nano-micron mineral matrix pores. The pore morphology in these samples is predominantly circular, with no obvious orientation (Fig. 11.e-f). The pore specific surface area, volume, and porosity exhibit higher values, averaging of 15.4 m²/g, 12.4 × 10⁻³ cm³/g, and 4.02%, respectively (Table 2).

The analysis indicates that strong tectonic compression negatively impacts pore development and preservation, significantly contributing to a decrease in pore structure parameters. Shale reservoir located further from zones of intense tectonic compression and fracturing exhibit preservation conditions and develop more favorable reservoir space. This is a crucial factor for shale gas enrichment and high production rates.

Burial depth
The analysis reveals a significant decrease in shale pore specific surface area and volume with increasing burial depth. Samples from the Zhaotong area (< 2000 m) exhibit the largest average pore specific surface area and volume, at 22.9 m²/g and 34.9 × 10⁻³ cm³/g, respectively. The Changning area (200–3500 m) follows, with averages values of 18.1 m²/g and 15.6 × 10⁻³ cm³/g, respectively. Samples from the Yuxi and Luzhou areas (> 3500 m) exhibit the smallest average pore specific surface area and volume, at 15.8 m²/g and 10.2 × 10⁻³ cm³/g, respectively. Interestingly, no significant relationship is observed between shale porosity and burial depth, with most values ranging from 3 to 6%. This suggests that high-quality pores can develop under diverse burial depth conditions (Fig. 12).
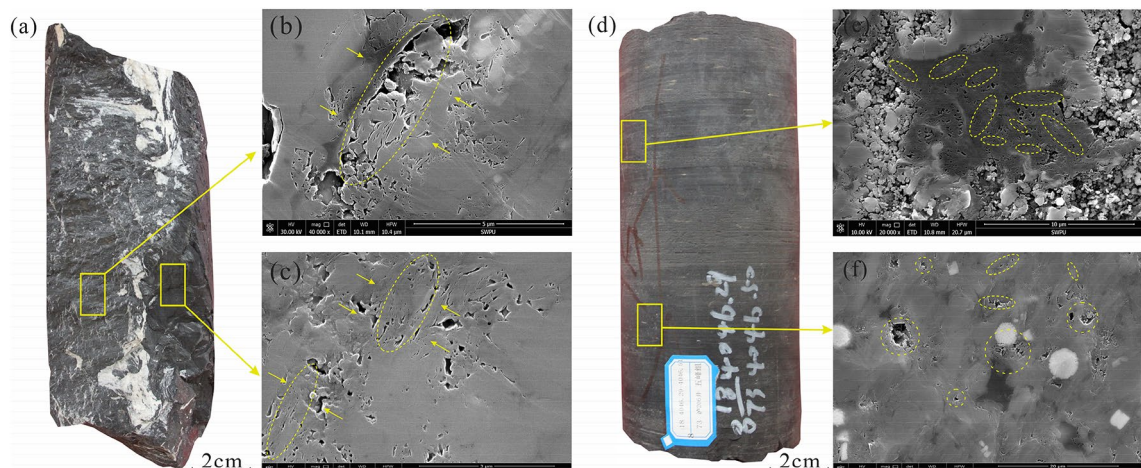
Fig. 11. Comparison of drill cores and microscale-reservoir space in different tectonic regions. (**a–c**) Well H203, located near the core of the anticline, exhibits multiple fractures at the macroscopic core scale, while the microscopic pore morphology displays an orientaion influenced by tectonic extrusion. (**d–f**) Well L206, located in the synclinal core, shows well-developed bedding at the core scale, and the microscopic reservoir space lacks a clear orientation.
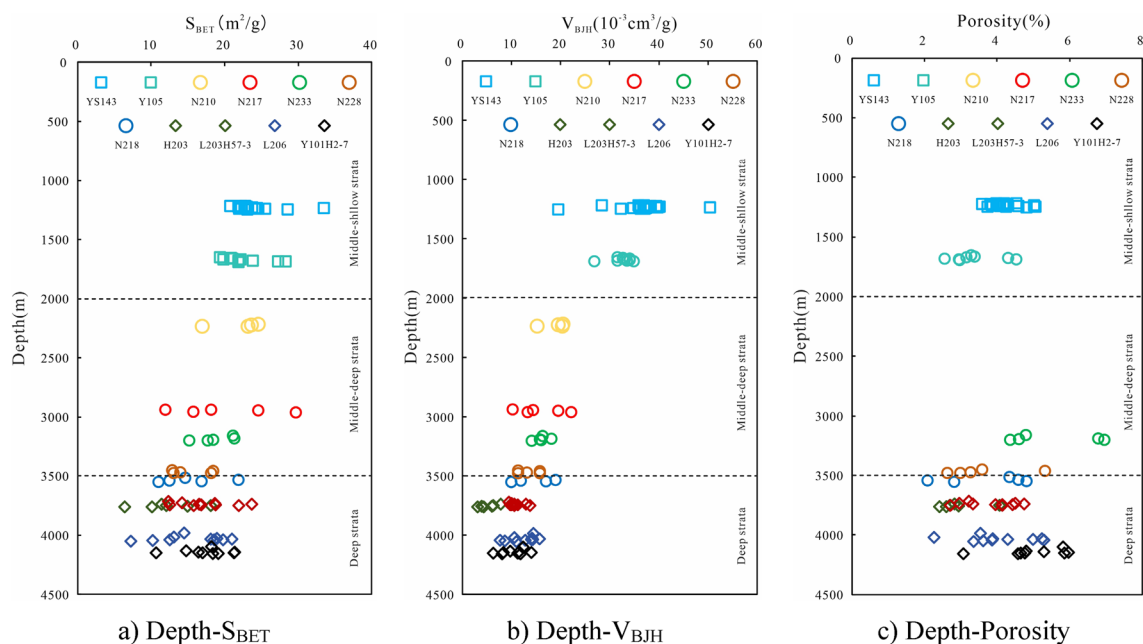

Fig. 12. Relationship between pore structure parameters(S_{BET}, V_{BJH}, and porosity) and burial depth (the squares represent samples from the Zhaotong area, the circle represent samples from the Changning area, and the diamond shape represent samples from the Yuxi and Luzhou areas).

This phenomenon can be attributed to the mitigating effect of factors such as the rigid framework composed of authigenic quartz particles and the presence of formation overpressure, which effectively offset compaction to some extent. This explains the minimal changes observed in porosity. However, the substantial compaction pressure exerted by overlying strata can still lead to pore closure, particularly affecting organic pores with small apertures and lacking rigid framework protection. The morphology of these pores tends to transition from ink-bottle shapes to slit-shaped configurations, resulting in a reduction in specific surface area and volume. When burial depth surpasses 3500 m, the formation's compaction resistance increase, diminishing the influence of burial depth on the pore structure, and slowing the declining trend in pore specific surface area and volume.

Conclusion

(1) The analysis revealed the presence of high-quality shale reservoirs at the base of the Longmaxi Formation in all four areas. However, regional variation in maturity, with the occurrence of local graphitization with high Ro values, can lead to a decline in reservoir quality, necessitating regional identification of such zones.

(2) Grey correlation analysis identified TOC content, Ro, tectonics, and burial depth as the most influential factors on pore structure, with the correlation coefficient of $0.72 \sim 0.76$, $0.73 \sim 0.74$, $0.65 \sim 0.71$ and $0.23 \sim 0.63$, respectively.

(3) The current study, finding a significant positive correlation between TOC content and pore structure parameters with no discernible threshold, indicates that confirming the existence of a threshold in the southern Sichuan Wufeng-Longmaxi shale demands further investigation with enhanced methodological diversity and broader sampling.

(4) The evolution of pore structure with increasing thermal maturity is governed by the co-evolution of organic and inorganic components. As organic matter advances from immature to overmature stages, the pore structure undergoes a six-stage progressive transformation, exhibiting a characteristic multi-phase evolutionary trajectory.

(5) Tectonic activity and significant burial depths were found to induce a transformation in shale pore morphology from ink-bottle shapes to slit-shaped configurations, leading to a reduction in specific surface area and pore volume.

Data availability

The datasets used and/or analysed during the current study available from the corresponding author on reasonable request.

References
1. EIA. *Drilling Productivity Report: for Key Tight Oil and Shale Gas Regions* (EIA Independent Statistics & Analysis, 2023).
2. Feng, Y. et al. Gas storage in shale pore system: A review of the mechanism, control and assessment. *Pet. Sci.* **20** (5), 2605–2636 (2023).
3. Zou, C. N. et al. Shale gas in china: characteristics, challenges and prospects(Ⅱ). *Pet. Explor. Dev.* **43** (2), 166–178 (2016).
4. Zou, C. N. et al. Development progress, potential and prospect of shale gas in China. *Nat. Gas. Ind.* **41** (1), 1–14 (2021).
5. Nie, H. K. et al. Graptolites zone and sedimentary characteristics of upper ordovician Wufeng formation-Lower silurian longmaxi formation in Sichuan basin and its adjacent areas. *Acta Petrolei Sinica.* **38** (2), 160–174 (2017).
6. Meng, G. M. et al. Pore characteristics and gas preservation of the lower cambrian shale in a strongly deformed zone. *North. Chongqing China Energies.* **15** (8), 2956 (2022).
7. Yang, T. et al. Prediction of total gas content in low-resistance shale reservoirs via models fusion - Taking the Changning shale gas field in the Sichuan basin as an example. *Geoenergy Sci. Eng.* **235**, 212698 (2024).
8. Wu, J. F. et al. Typical types of shale gas reservoirs in Southern Sichuan basin and enlightenment of exploration and development. *Nat. Gas Geoscience.* **34** (8), 1385–1400 (2023).
9. He, X. et al. Accumulation conditions and key exploration and development technologies of marine shale gas field in Changning-Weiyuan block, Sichuan basin. *Nat. Gas. Ind.* **42** (2), 259–272 (2021).
10. Li, J. et al. Geological characteristics and three-dimensional development potential of deep shale gas in the Luzhou Area, Southern Sichuan basin, China. *Journal of Geo-Energy and Enviroment.* **1** (1), 32–44 (2025).
11. Ren, G. et al. Quantitative assessment of shale gas preservation in the Longmaxi Formation: Insights from shale fluid properties. *Journal of Geo-Energy and Enviroment.* **1** (1), 8–22 (2025).
12. Jacob, H. Classification, structure, genesis and practical importance of natural solid oil bitumen ("migrabitumen"). *International Journal of Coal Geology.* **11** (1), 65–79 (1989).
13. Chen, G. S. et al. New Understandings of the factors controlling of deep shale gas enrichment in the Wufeng formation-Longmaxi formation of the Southern Sichuan basin. *Nat. Gas. Ind.* **44** (1), 58–71 (2024).
14. Wang, X. Q. *Study on Shale Gas Accumulation Process and Enrichment Mechanism of Wufeng-Longmaxi Formation in Changning Area* (China University of Mining and Technology, 2021).
15. Milliken, K. L. et al. Organic matter–hosted pore system, Marcellus formation (Devonian), Pennsylvania. *AAPG Bull.* **97** (2), 177–200 (2013).
16. Hammes, U. et al. Geologic analysis of the upper jurassic Haynesville shale in East Texas and West Louisiana. *AAPG Bull.* **95** (10), 1643–1666 (2011).
17. Romero-Sarmiento, M. F. et al. Evolution of barnett shale organic carbon structure and nanostructure with increasing maturation. *Org. Geochem.* **71**, 7–16 (2014).
18. Brunauer, S. et al. Adsorption of gases in multimolecular layers. *J. Am. Chem. Soc.* **60** (2), 309–319 (1938).
19. Li, H. et al. Quantitative analysis of pore complexity in lacustrine organic-rich shale and comparison to marine shale: insights from experimental tests and fractal theory. *Energy Fuel.* **38** (17), 16171–16188 (2024).
20. Li, J. et al. Shale pore characteristics and their impact on the gas-bearing properties of the longmaxi formation. *Sci. Rep.* **14**, 16896. 2024 (2024).
21. IUPAC (International Union of Pure and Applied Chemistry). Physical chemistry division commission on colloid and surface chemistry, subcommittee on characterization of porous solids: recommendations for the characterization of porous solids. *Pure Appl. Chem.* **66** (8), 1739–1758 (1994).
22. Wang, K. et al. Methane and CO_2 sorption hysteresis on coal: A critical review. *Int. J. Coal Geol.* **132**, 60–80 (2014).
23. Leng, Y. J. et al. Shale hydration and its influencing effect on water phase flowback: a case of longmaxi formation in Weiyuan area, Sichuan basin. *J. Cent. South. Univ. (Science Technology).* **53** (9), 3681–3693 (2022).
24. Deng, J. L. Grey control system. *J. Huazhong Univ. Sci. Technol. (Natural Sci. Ed.)* **3**, 9–18 (1982).
25. Tu, Y. et al. Evaluation criteria and classification of shale gas reservoirs. *Oil Gas Geol.* **35** (1), 153–158 (2014).
26. Chen, Y. et al. Pore structure heterogeneity of deep marine shale in complex tectonic zones and its implications for shale gas exploration. *Energy Fuels.* **38** (3), 1891–1905 (2024).

27. Liu, W. P. et al. Controlling factors and evolution laws of shale porosity in longmaxi formation, Sichuan basin. *Acta Petrolei Sinica*. **38** (2), 175–184 (2017).
28. Chen, Y. et al. Analysis of shale pore characteristics and controlling factors based on variation of buried depth in the longmaxi formation, Southern Sichuan basin. *Geol. China*. **49** (2), 472–484 (2022).
29. Tang, H. M. et al. Pore structure difference of shale in different structural units and its petroleum geological implications: A case study on deep shale in the Luzhou area, Southern Sichuan basin. *Nat. Gas. Ind*. **44** (5), 16–28 (2024).
30. Cao, T. T. et al. Characterizing the pore structure in the silurian and permian shales of the Sichuan basin, China. *Mar. Pet. Geol*. **61**, 140–150 (2015).
31. Song, D. J. et al. Research progress on nanoscale pore structure characteristics of organic-rich shale. *Acta Sedimentol. Sin*. **37** (6), 1309–1324 (2019).
32. Li, H. et al. Pore structure evolution and geological controls in lacustrine shale systems with implications for marine shale reservoir characterization. *Sci. Rep*. **15**, 17702 (2025).
33. Yu, W. M. et al. Experimental study on the existence of nano-scale pores and the evolution of organic matter in organic-rich shale. *Nanatechnol. Reviews*. **8** (1), 156–167 (2019).
34. Wang, Y. *Nanoscale Pore Structure Evolution and Shale Gas Occurrence of Longmaxi Formation in Upper Yangtze Area* (China University of Mining and Technology, 2018).
35. Cheng, P. et al. Water content and equilibrium saturation and their influencing factors of the lower paleozoic overmature Organic-Rich shales in the upper Yangtze region of Southern China. *Energy Fuels*. **32** (11), 11452–11466 (2018).
36. He, D. F. et al. Formation and evolution of Sichuan polycyclic superimposed basin. *Chin. J. Geol. (Scientia Geologica Sinica)*. **46** (3), 589–606 (2011).

Author contributions
Yijiang Leng: Conceptualization, Methodology, Writing – original draft, Writing – review & editing. Hongming Tang: Conceptualization, Methodology, Supervision. Yutian Feng: Conceptualization, Methodology, Investigation. Xuewen Shi: Resources, Data curation. Weiming Yu: Resources, Data curation. Zeyan Li: Writing –review & editing, Data curation.Hu Li: review & editing, Data curation.

Funding

Declarations

Competing interests
The authors declare no competing interests.

Additional information
Correspondence and requests for materials should be addressed to H.T.

Reprints and permissions information is available at www.nature.com/reprints.

Publisher's note Springer Nature remains neutral with regard to jurisdictional claims in published maps and institutional affiliations.